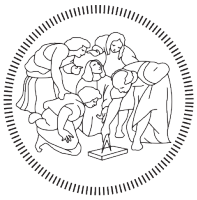

POLITECNICO
MILANO 1863

Liquid Rocket Engine Preliminary Design

Pietro Bosco (10643020), Tommaso Brombara (10682041), Riccardo Cadamuro (10702567), Álvaro Flórez González (10911708), Emanuele Marzorati (10724126), Daniele Peruzzotti (10702005)

- pietro1.bosco@mail.polimi.it
- tommaso.brombara@mail.polimi.it
- riccardo.cadamuro@mail.polimi.it
- alvaro.florez@mail.polimi.it
- emanuele.marzorati@mail.polimi.it
- daniele.peruzzoti@mail.polimi.it

KiSS group

Course of Space Propulsion
School of Industrial Engineering
Academic Year 2022-2023

Nomenclature

Symbol	Definition	Unit
A	Area	m^2
A_c	Chamber Area	m^2
A_e	Exit Area	m^2
A_t	Throat Area	m^2
c^*	Characteristic Velocity	m/s
C_d	Discharge coefficient	[-]
C_p	Specific heat	$Jkg^{-1}K^{-1}$
CR	Contraction Ratio	[-]
D_{cc}	Combustion Chamber Diameter	m
D_{inj}^{fu}	Fuel Injector Diameter	m
D_{inj}^{Ox}	Oxidizer Injector Diameter	m
ΔP	Delta Pressure	Pa
ΔT	Delta Temperature	K
ΔV	Delta Velocity	m/s
H	Thermal Resistance	KW^{-1}
h_c	Convection Coefficient	$Wm^{-2}K^{-1}$
I_s	Specific Impulse	s
k	Thermal Conductivity	$Wm^{-1}K^{-1}$
L^*	Characteristic Length	m
L_{cc}	Combustion Chamber Length	m
m_0	Inert mass budget	kg
m_{fu}	Fuel Mass	kg
m_{ox}	Oxidizer Mass	kg
m_{he}	Helium Mass	kg
M_e	Mach at exit	[-]
$\dot{m}_{fu}$	Fuel Mass Flow Rate	kg/s
$\dot{m}_{ox}$	Oxidizer Mass Flow Rate	kg/s
N_{fu}	Number of fuel injector holes	[-]
N_{ox}	Number of oxidizer injector holes	[-]
Nu	Nusselt Number	[-]
O/F	Oxidizer to Fuel ratio	[-]
P_c	Chamber Pressure	Pa
P_e	Pressure at exit	Pa
Pr	Prandtl Number	m^2s^{-1}
$\dot{Q}$	Heat Flux	W
Re	Reynolds Number	[-]
T	Thrust	N
t_b	Burning Time	s
V_{cc}	Combustion Chamber Volume	m^3
a	Sonic Velocity	m/s
m_s	Inert mass budget	kg
α	Impingement angle	$degrees$
λ	Nozzle Correction Factor	[-]
ϵ	Expansion Ratio	[-]

Contents

List of Tables

Chapter 1

Introduction

The purpose of this paper is to submit an overview of a preliminary design of a liquid propellant kick stage motor for a small satellite. The spacecraft shall be able to perform an orbital transfer which requires a $\Delta V = 2500\frac{m}{s}$ considering an inert mass budget $m_0 = 250kg$. Pressure and thrust level are constant.
The layout of the engine is the result of a trade-off between propellant weight, compactness, compatibility of components/propellants, and production feasibility. This dossier will examine different engines basing on two main factors:

- Propellants couple: the choice is between a green (low toxic) propellant and a standard design based on hydrazine and nitrogen tetroxide, which is highly dangerous and problematic to handle. In both cases, the propellant is supposed to be storable;
- Thrust level: different scales of engine are considered. More specifically, the comparison stands on doubling and halving the thrust level with respect to the nominal size

Furthermore, regarding the method of construction of the engine, the injector plate and engine casing are meant to be constructed as a monolithic unit through the use of metallic additive manufacturing technologies, with the goal of reducing mass and cost per unit.
This dossier shall present an exploratory, yet representative model of a pressure-fed, bipropellant liquid propulsion system, starting from the sizing of the tanks and the feeding lines to the design of the thrust chamber and the nozzle. Moreover, the choice of the material is crucial; this decision not only deals with the capacity to withstand high pressures and temperatures and with the compatibility with the propellants, but also with the feasibility with additive manufacturing relating to the construction of both the case and the injection plate.
The goal is to aid in the comparison of the two propellant types, as well as to analyze the possibility of scaling the thrust level of the engine.

Chapter 2

State-of-the-Art

2.1 Kick stages use and development

The development of commercial space activities has imposed new dynamics and challenges on the space transportation industry. Multi-injection capabilities and in-orbit services will become key features for any launcher provider in the upcoming decades. Kick stages are space vehicles designed to provide the last-mile delivery after dedicated, rideshare or piggyback launches, and cover a crucial role in orbital deployment and attitude control. Placing small satellites into various target orbits from a single launch is rapidly becoming a mandatory feature in many agencies future projects, as well as using storable propellants in order to do so.
The current focus in on the development of a safer, non-toxic propellant combination, commonly referred to as GREEN propellants, in order to phase out Hydrazine and reduce personnel training and handling costs, while providing similar performances in terms of specific impulse.
A perfect example lies on the BERTA project [1], which is being promoted by ESA and ArianeGroup aiming to deliver a kick-stage engine for the future Ariane 6 rocket.

2.2 Green propellant development

Hydrazine and oxides of nitrogen have been the fundamental propellants for chemical space propulsion since its early developments. Nowadays the most widely used storable propellant combination employed in the design of liquid upper stages and kick stages is the hypergolic couple Hydrazine (or some derivatives such as UDMH and MMH) and NTO, whose use begun in the early 60s as storable fuel for ICBMs and is still in use today as a reliable and efficient propellant.
In contrast Hydrazine's biggest drawback is its extreme toxicity, however the high specific impulse that can be achieved by using it makes it one of the best alternatives as a storable propellant.
Due to their intrinsic problems, mentioned above, the recent research trend in space propulsion is directed into green technologies.
Moreover, research on green alternatives is based on the avoidance of expensive solutions used nowadays. Propellant ought to be easy to handle. It means that low vapour pressure is also desired. To compare, hydrazine vapour pressure equals to 1.92 kPa at 25^{o}C. In the case of hydrogen peroxide, it is 0.26 kPa at the same temperature. In bipropellant mode, performance of peroxide based propulsion and conventional storable oxidizer/fuel

configurations are comparable. Furthermore, volumetric specific impulse of all green propellant configurations using 98% HTP is, in general, higher than these based on hydrazine. These significant aspects make hydrogen peroxide one of the most promising green oxidizers. Some problems to consider are its availability, still hard, due to very demanding production process, and its challenging long term storability [2]. Some of the most promising green options as fuels are light hydrocarbons, kerosene and alcohols which are all less toxic than hydrazine and used with HTP98% have performance parameters (figure 2.1) similar to UDMH-NTO [3]. They still require careful handling, since they are especially flammable and show some risk of explosions if heated. [4]

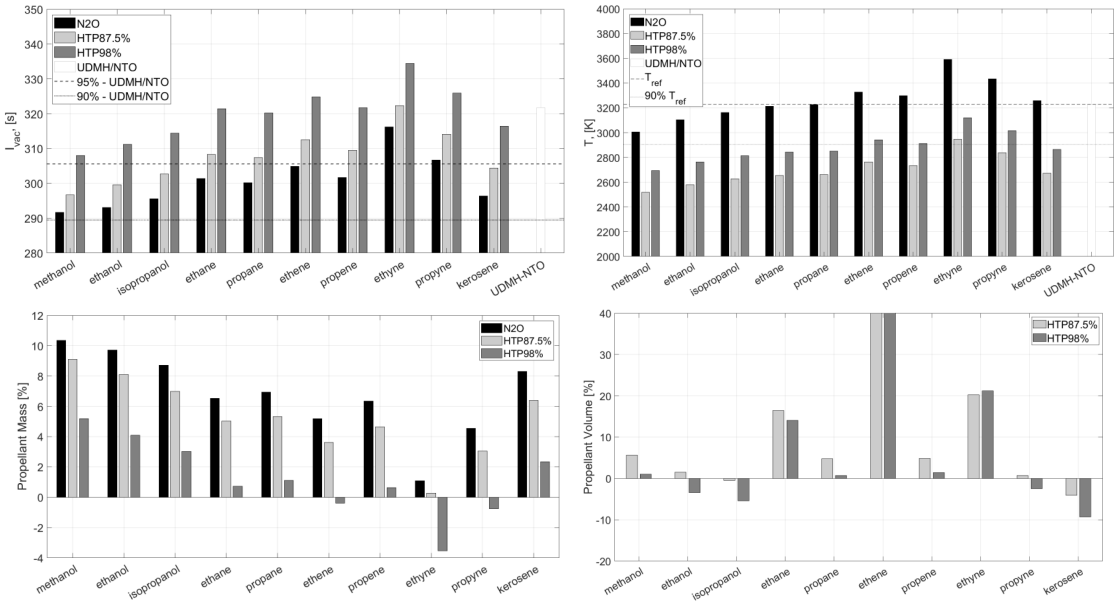

Figure 2.1: Performance of green alternatives compared to UDMH-NTO

2.3 Metal compatibility with propellant

An important consideration in the design of spacecraft for interplanetary missions is the compatibility of storage materials with the propellants. Serious problems can arise because many propellants are either extremely reactive or subject to catalytic decomposition, making the selection of proper materials of construction for propellant containment and control a critical requirement for the long-life applications. In order for a metal to be considered compatible with a propellant, corrosion must be negligible and no increase in decomposition rate of the latter should be noted.
The propellants this literature review is focusing on are Hydrazine, Nitrogen tetroxide, RP-1 and Hydrogen peroxide. Tables (2.1) and (2.2) show their compatibility with some of the most used or promising materials [5] [6] [7] [8] [9] [10] [11] [12].

Material	N2H4	N2O4	RP-1	H2O2 98%
Al5052	compatible	compatible	compatible	compatible
Al5254	NA	compatible	compatible	compatible
SS304L	compatible	compatible	NA	NA
SS304	compatible	conflicting data	compatible	compatible
Ti-6Al-4V	compatible	compatible	NA	not compatible

Table 2.1: Possible tank and lines materials

Material	N2H4	N2O4	RP-1	H2O2 98%
Inconel X750	compatible	NA	compatible	compatible
Inconel 718	compatible	compatible	compatible	compatible
Rhenium	compatible	compatible	NA	NA
Niobium c-103	compatible	compatible	NA	NA

Table 2.2: Possible thrust chamber and injector materials

For the propellant tanks material there are a few different choices, such as Ti-6Al-4V, Al5052 and SS304L for the toxic couple, and Al5052, Al5254 and SS304 for the non-toxic one. For the thrust chamber and injector the certainly compatible materials are Inconel X750 and Inconel 718 for the non-toxic couple and Inconel 718, Rhenium and Niobium C-103 for the toxic one.

2.4 Metal compatibility with additive manufacturing

Having taken the affinity of the materials with the propellants into account, a further selection should be done checking the possibility of performing additive manufacturing, regarding to the need to build the case and the injection plate in one single block; that is illustrated in Table (2.3).

Material	Printability
Inconel X750	NA
Inconel 718	compatible
Rhenium	NA
Niobium c-103	compatible

Table 2.3: Material compatibility with additive manufacturing techniques

The compatibility with additive manufacturing is assured for Inconel 718 and Niobium C-103. For the manufacturing of this particular thruster, Selective Laser Melting (SLM) was chosen as the manufacturing process; more specifically, the SLM®2 Selective Laser Melting printer [13], capable of printing with powdered Inconel 718. Specific properties of the printer are shown in Table (2.4).

Build envelope [mm]	Minimum size feature [μm]	Beam focus diameter [μm]	Dimensional accuracy [μm]	Variable layer thickness [μm]	Smallest hole feature [mm]
280 x 280 x 365	150	80 - 115	$\geq$ 50	20 - 90	0.762

Table 2.4: SLM®280 specifications

This printer has been selected due to its low minimum feature size and resolution, which provides great flexibility on the design of components that are critical from the manufacturing accuracy point of view [14].

Chapter 3

Requirements

The nominal thrust level of the engine has been picked to be equal to 700N.

This design choice has been made on the basis of the role, Δv requirement, and inert spacecraft mass, as the longer the burn time of the engine (i.e. the lower the thrust level), the further away from the impulsive model we get. This implies that the Tsiolkovsky equation used to compute the propellant mass required to guarantee the $2500\frac{m}{s}$ Δv for the mission will get more and more imprecise due to losses related to the change of position and angle between the orbital path and thrust direction.
One further consideration has been made related to the assigned inert mass: the engine shall be kept at a reasonable scale to make sure that the weight of the engine, feeding lines and tanks is compliant with the final inert mass; another aspect was to choose a thrust level such that the maximum acceleration perceived by the payload during the propulsive phase would not exceed the ones of the launch, therefore not imposing any further constraints on its structure. This result is in line with other engines that fit the same category of the one being designed here.
Non-nominal designs will present thrust levels of 350 and $1400N$ to analyze the feasibility of scaling the engine designs found to different factors in order to expand the production pool and possible uses for the design.

3.1 Material selection

For the purpose of the paper Inconel 718 has been selected, despite the superior characteristics of Rhenium and Niobium, due to its easier and more reliable printability and the extensive literature and practical applications regarding its use in the construction of high performance combustion chambers. Also, current prices for the raw product are far lower than its competitors, especially Rhenium.
This choice fix the maximum operating temperature, on the inside of the wall of the combustion chamber at $900K$. Moreover it appeared to be necessary a further ceramic layer, in order to shield and isolate the Inconel wall, as well as lowering the heat flux towards the coolant liquid. The selected ceramic is Porous Mullite doped with microdosed ZrO2 and WO3. This solution is characterised by an extrimely low thermal conductivity, less than 0.5 W/mK at 1100°C, and capable to withstand temperature high as much as 1300°K. ([15])

3.2 Cooling

The engine design must be capable of being cooled through the use of regenerative cooling, without incurring into boiling or thermal decomposition of the cooling fluid employed, the compatibility between fluid and cooling jacket pipes must be accounted as well.
The section of interest for this paper is the combustion chamber and throat area, as in the divergent section other forms of cooling, such as radiative cooling, can be employed. If this is found not to be possible, either a film cooling or an extra layer of refractory material must be applied in order to reduce the maximum temperature of the metal to the specified one. In this paper particular case of study, the use of Mullite Ceramic lowered the temperature of the coolant by 50°- 60°.
Moreover injector design and impingement point were chosen in order to avoid strong thermal effects on the injector plate.

3.3 Toxic couple

For the analysis of the engine fueled by the toxic couple N2H4/N2O4, some initial requirements, in Table (3.1), have been fixed based on available literature and already working engines. [16]

Chamber Pressure [bar]	10
Expansion ratio ϵ	130
L* [m]	0.75
CR	8
Maximum wall temperature [K]	900

Table 3.1: Toxic couple design requirements

O/F ratio has been derived from an optimization process aimed at maximising the specific impulse and cooling capability.
The result of the optimisation returns the following parameters:

O/F	0.9346
I_s[s]	348,7
$I_v[\frac{kg \cdot s}{m^3}]$	$4.122 \cdot 10^5$
$c^*[\frac{m}{s}]$	1858,3
C_T	1.8406

Table 3.2: Performance parameters obtained through CEA optimization

3.4 Green alternative

For the H2O2/RP-1 engine the choice fell on the design of an engine based on the [17] catalytic decomposition of H2O2 on a bed of catalyst prior to chamber injection[18] [19]. Main requirements fixed in the design phase are shown in Table (3.3).

Chamber Pressure [bar]	10
Expansion ratio ϵ	130
L* [m]	1.52
CR	8
Maximum wall temperature [K]	900
Catalyst material	Mn_xO_y (3.5 mm pellets, Alumina substrate)

Table 3.3: Green couple design requirements

O/F ratio has been derived from an optimization process aimed at maximising the specific impulse and cooling capability.
The result of the optimisation returns the following parameters:

O/F	5,9156
I_s[s]	323,2
$I_v[\frac{kg \cdot s}{m^3}]$	$4.1643 \cdot 10^5$
$c^*[\frac{m}{s}]$	1653,2
C_T	1,9180

Table 3.4: Performance parameters obtained through CEA optimization

Chapter 4

Design and results

The design process is based on the NASA-CEA code to compute the thermodynamic properties of the reactants and their thermal behaviour. In particular, the team assumed an equilibrium reaction until the throat section while, from that point to the exit, the flow is considered frozen.
This configuration has been chosen because it generally produces results that well approximates the actual operating behaviour of an engine.

4.1 Nozzle Design

The conical nozzle is the least performing one due to the 2D losses on the divergent part. In order to find a trade-off between the minimization of these losses with its length, it appeared to be necessary the use of the RAO approximation, considering $L_{RAO} = 0.8L_{ref}$, which is a widely used value.
By correlating the expansion ratio (ϵ) to the initial and final angle of RAO's parabola, it is possible to compute the divergency loss factor and the nozzle length.
In order to compute RAO's nozzle parameter it is necessary to know also the throat area that is computed to provide the required thrust level in the given thermal condition.
By simulating with the CEA code the combustion at a fixed chamber pressure p_C, it is possible to obtain the c^* and the pressure, Mach number and speed of sound at the nozzle exit, respectively: p_e, M_e and a_e. At this point by recalling the c^* definition:

$$c^* = \frac{p_C \cdot A_t}{\dot{m}_P} \tag{4.1}$$

and the thrust equation:

$$T = \lambda(A_t) \cdot \dot{m}_P v_e + p_e A_e \tag{4.2}$$

where:

$\lambda(A_t)$ represent the implicit fuction that correlates the throat area with the divergency-loss factor;

v_e is the flow exit velocity

A_e is the exit area

it is possible to solve numerically the following implicit equation to compute A_t:

$$T - \lambda(A_t) \cdot \frac{p_C \cdot A_t}{c^*} \cdot M_e a_e + p_e A_t \epsilon = 0 \tag{4.3}$$

and, once computed A_t it is also possible to compute the mass flow rate $\dot{m}_P$ according with (4.1) leading to the following results:

Propellant	$A_t[\ m^2]$	ϵ	$L; Nozzle[\ m]$	λ	$theta_I[\ deg]$	$theta_E[\ deg]$	$\dot{m}_P[\frac{kg}{s}]$
N2H4/N2O4	$3.8 \cdot 10^{-4}$	130	0.342	0.985	37°	9°	0.205
H2O2/RP-1	$3.6 \cdot 10^{-4}$	130	0.334	0.985	37°	9°	0.221

Table 4.1: Nozzle data

4.2 Combustion Chamber Design

The main parameter of merit which identifies the combustion chamber is the characteristic length L*; its value can be obtained from the literature. Table (4.2) shows L* values for different propellant combinations [20].

Propellant combination	L* [cm]
Nitric acid/hydrazine-base fuel	76-89
Nitrogen tetroxide/hydrazine-base fuel	76-89
Hydrogen peroxide/RP-1 (including catalyst bed)	152-178
Liquid oxigen/RP-1	102-127
Liquid oxigen/ammonia	76-102
Liquid oxigen/liquid hydrogen(GH_2 injection)	56-71
Liquid oxigen/liquid hydrogen(LH_2 injection)	76-102
Liquid fluorine/liquid hydrogen(GH_2 injection)	56-66
Liquid fluorine/liquid hydrogen(LH_2 injection)	64-76
Liquid fluorine/hydrazine	61-71
Chlorine trifluoride/hydrazine-base fuel	51-89

Table 4.2: Characteristic length for the main propellant combinations

The chamber is supposed to be shaped as a cilinder with constant section area: knowing the throat area from 4.1 and having set the contraction ratio (A_c/A_t) to 8 (acceptable value according to the literature), the combustion chamber has been sized and the results are shown in Table (4.3).

Propellant	$L^*[m]$	$L_{cc}[m]$	$D_{cc}[m]$	$V_{cc}[cm^3]$
N2H4/N2O4	0.75	0.0838	0.0622	285.2
H2O2/RP-1	1.52	0.1803	0.0608	524.3

Table 4.3: Combustion chamber sizing results

Since the NASA-CEA only outputs total values of temperature, pressure and density in the combustion chamber section, the static one have been computed through the previous computation of the Mach number in the chamber by satisfying the continuity equation.

$$\dot{m}_F = \rho_F A_C v_C \tag{4.4}$$

but ρ_F needs to be converted from being a total to a static quantity as:

$$\begin{cases} {\rho_F}^S = {\rho_F}^T \left(1 + \frac{\gamma-1}{2} M^2\right)^{\frac{1}{\gamma-1}} \\ M = \frac{v_C}{a_C} \end{cases} \tag{4.5}$$

that leads to the following equation that can be solved for v_C

$$v_C - \frac{\dot{m_F}}{A_C {\rho_F}^T \left(1 + \frac{\gamma-1}{2} \frac{{v_C}^2}{a_C}\right)^{\frac{1}{\gamma-1}}} = 0 \tag{4.6}$$

allowing the computation of the Mach number in the combustion chamber and the complete set of static quantities.

4.3 Propellant mass

The propellant mass is calculated using through the Tsiolkovsky rocket equation:

$$m_p = m_s \cdot (e^{\frac{\Delta v}{I_{sp} \cdot g_0}} - 1) \tag{4.7}$$

where the specific impulse has been obtained by the NASA CEA code, assuming unitary efficiency for both η_{c^*} and η_{C_T}.
The operative OF ratio has instead been computed through an optimization process that aims to maximize the engine specific impulse but with the constraints of not heating over the boiling point or decomposition point the fuel in the cooling circuit.
The fuel and oxidizer masses are then calculated as:

$$\begin{cases} m_{Fu} = \dfrac{m_p}{1 + O/F} \\ m_{Ox} = O/F \cdot m_{Fu} \end{cases} \tag{4.8}$$

Knowing the density of the propellants and the mass flow rate, the volume and burning time are obtained. The results are shown in Table (4.4).

Propellant	m_p [kg]	O/F [-]	m_f [kg]	m_o [kg]	V_f [m^3]	V_o [m^3]	t_b [s]
N2H4/N2O4	269.25	0.9347	139.17	130.08	0.1318	0.0897	1316
H2O2/RP-1	332.06	5.9016	41.50	290.51	0.0159	0.2022	1403

Table 4.4: Results of the propellant mass sizing

4.4 Injection Plate Design

Both the oxidizer and the fuel have been assumed to enter into the injectors in liquid form. Regarding the green couple, a catalytic bed would be necessary in order to have a more efficient reaction in the combustion chamber: that would work by making the hydrogen peroxide decompose into water, oxygen and heat before it reaches the injector, making the reaction between the oxidizer and the fuel much more likely to start sooner once in the chamber.
The discharge coefficient C_d is dependent on the geometry of the injection inlet. In fact,

the choose for our injectors a sharped-edge cone geometry which gives us this previous value of 0.7 for both the fuel and the oxydizer.
The minimum injector diameter has been set to $0.762mm$ based on the current additive manufacturing capabilities.
The total injection area for both fuel and oxidizer has been computed as:

$$A_{inj} = \frac{\dot{m}}{C_d\sqrt{2\Delta p_{inj}\rho}} \tag{4.9}$$

The number of injector for both fuel and oxidizer has been computed from the total area required by ensuring each injector to have a section greater than the minimum one satisfying the required ratio between oxidizer and fuel ones, and to satisfy the injection geometry chosen.
The initial data is defined in Tab(4.5).

Propellant	$\dot{m}_{fu}[kg/s]$	$\dot{m}_{ox}[kg/s]$	C_d
N2H4/N2O4	0.1058	0.0989	0.7
H2O2/RP-1	0.0269	0.2070	0.7

Table 4.5: Initial data

For the toxic propellant couple, a like-on-like configuration has been chosen. As a matter of fact, hydrazine N_2H_4 and dinitrogen tetroxide N_2O_4 are an hypergolic couple whose components spontaneously ignite when they come into contact with each other. This configuration offers less effective mixing and atomization.

To start sizing, we defined a nominal pressure drop occurring during the injection [21] of

$$\Delta P = 30\%P_c \tag{4.10}$$

In this case there is no relation between the number of oxidizer injectors and fuel ones, but them both shall be even.

The impingement point is located at a distance of 5 mm from the injection head and the impingement angle has been assumed to 30 deg, with the two injectors spaced $2.9mm$ apart [22].

For the green case, triplets injectors were chosen due to the difference in total areas of injection needed. The angle of the fuel injector is set to 0 deg, spraying straight into the combustion chamber, while two oxidizer injectors placed $4mm$ to the sides of the fuel, one spray into the fuel stream at an angle of 45 deg, the maximum overhang angle currently achievable through metallic AM, to generate an impingement point $4mm$ away from the injector plate [22].
The goal is to mix the two propellants rapidly, as their reaction speed is slower than for the toxic, hypergolic case. We cannot, however, put the holes too close together as not to compromise the structural integrity of the injector plate.

Propellant	$D_{inj}^{Fu}[mm]$	$D_{inj}^{Ox}[mm]$	N_{Fu}	N_{Ox}	$\alpha_{Fu}[deg]$	$\alpha_{Ox}[deg]$	$v_{inj}^{Fu}[\frac{m}{s}]$	$v_{inj}^{Ox}[\frac{m}{s}]$
N2H4/N2O4	0.81	0.87	12	8	30	30	17	14
H2O2/RP-1	0.81	5.67	4	8	0	45	19	14

Table 4.6: Nominal Injectors Sizing

Note that the large size of H_2O_2 injector size is due to the fact that the peroxide is decomposed by the catalyst into heated steam and oxygen which has a low density compared to the liquid fuel.
Referring to the injection velocity, the fuel velocity seems to be in an acceptable range according to the literature, while the oxidizer velocity is quite low. In the first case the propellant is hypergolic, minimizing indeed the mixture and atomization problems while, in the other case, it is in gas state.

4.5 Cooling Design

For the scope of this paper only the cooling strategy of the combustion chamber, convergent section, and throat section of the nozzle has been considered. It is assumed that radiative cooling would be employed in the divergent section of the nozzle.
The cooling system relies on a regenerative strategy, chamber contraction ratio and oxidizer over fuel ratio have been sized in order to ensure the possibility to absorb through the thermal capacity of the fuel, the heat flux coming from the combustion chamber and the convergent part of the nozzle. The problem has been modeled as follows:
First the number of Nusselt has been computed through Dittus-Boelter relation

$$Nu = 0.0265 Re^{0.8} Pr^{0.3} \tag{4.11}$$

This relation is in general valid for $Pr > 0.6$ and $Re > 10000$, conditions that were found to be verified. Even though better approximation exists, this relation provide anyways a good estimation. Subsequently the convection coefficient is computed through the Nusselt definition and from that the heat flux exiting a given section is set equal to the one absorbed by the fuel.

$$h = \frac{k}{L} \cdot Nu \tag{4.12}$$

$$\dot{Q}_{exit} = h \cdot A \cdot (T_{flame} - T_{wall}) \tag{4.13}$$

$$\dot{Q}_{abs} = \dot{m_F} \cdot C_P \cdot (T_{out} - T_{inp}) \tag{4.14}$$

In some cases where the fuel thermal capacity was not enough to absorb the heat flux without boiling, a second regenerative stage based on the use of oxidizer to remove the exceeding heat flux has been considered. One of the fluids cools the area from the injector plate to a point downwards, the other from the throat section upwards. In the last case particular attention has been posed in avoiding the oxidizer to reach high temperatures to avoid it becoming reactive or to disassociate [23].
Boiling points have been estimated through the Clausius-Clapeyron equation for a limiting condition equal to the lowest pressure achieved at the end of the cooling loop.
One further step has been made through adding a coating layer inside the combustion chamber based on Mullite, a ceramic material, doped with microdosed ZrO2 and WO3.

Material	$k_{shield}[W/mk]$	$MaximumWorkingTemperature[K]$
Mullite	0.5	1300

Table 4.7: Ceramic Shield Material Properties

In this case the coating thickness is computed in order to preserve the total heat flux and to have the two interface surfaces at their maximum operative temperature.

$$x_{th} = \frac{k}{h_c} \cdot \left(\frac{\Delta T_1}{\Delta T_2} - 1 \right) \tag{4.15}$$

where:

k represents the thermal conductivity of the coating material

h_c represents the convection coefficient

$\Delta T_1 = T_{flame} - T_{wall}$

$\Delta T_2 = T_{flame} - T_{coat}$

At this point it is possible to compute the new thermal resistance H:

$$H = \frac{1}{\frac{1}{h_c} + \frac{x_{th}}{k}} \tag{4.16}$$

such that:

$$\dot{Q} = H \cdot A \cdot (T_{flame} - T_{wall}) \tag{4.17}$$

The insertion of this ceramic coating was necessary in the green propellant-fed engine, while the toxic based one does not require it. Moreover the scaled down versions always require it because of the very low propellant mass flow rate compared with the heat flux to dissipate.

Propellant	$T_{Ox}[\ K]$	${T_{Ox}}^{limit}[\ K]$	$T_{Fu}\ [K]$	${T_{Fu}}^{limit}[\ K]$	${x_{th}}^{coat}[\ mm]$
N2H4/N2O4	296	350	435	460	-
H2O2/RP-1	389	423	428	482	0.185
H2O2/RP-1	410	423	428	482	-

Table 4.8: Coolant temperatures

As can be seen in tab 4.8, in the green based engine (H2O2/RP-1) without the ceramic coating, the peroxide reaches a temperature close the boiling point, making it unfeasible. A thin layer of Mullite can significantly increase the safety margin by increasing the separation between the maximum fuel temperature and its decomposition point[23].

4.6 Feed Lines

The feeding system consists in two separate lines, one for the oxidizer and one for the fuel. In order to properly model the feed line, both concentrated and distributed losses are taken into account. The absolute roughness coefficient k for aluminium has been taken as 0.002 mm [24] and the pressure drop from the cooling jacket has been taken as 25% of the chamber pressure. Also the effect of concentrated loss has been taken into account, in particular the total loss has been estimate as 1.25 bar for each line that consists in around 1.1 bar for a control valve and 0.15 bar for the check valve [25].
The pipes maximum length has been computed in order to ensure a maximum distributed

loss along the line equal to 0.20 *bar*, while the diameter has been sized according with the production standard (i.e. 1/4") and with the mass flow rate to obtain a flow velocity between 1 and 10 m/s.
The total pressure drop, maximum length and radius of the pipe of the two lines are shown in table (4.9), assuming that both fluids run through the cooling loop and are subject to the related pressure drop.

N2H4/N2O4	$\Delta P_{feed+cooling}$ [bar]	Radius [mm]	Max Length [m]
Oxidizer	3.95	3.2	24.9
Fuel	3.95	3.2	8.68

H2O2/RP-1	$\Delta P_{feed+cooling}$ [bar]	Radius [mm]	Max Length [m]
Oxidizer	3.95	3.2	4.45
Fuel	3.95	3.2	28.9

Table 4.9: Feed line characteristics

4.7 Tanks Design

The tanks have been designed to be compliant with the pressure loss along the lines in order to guarantee the correct pressure at injection since the system is to be considered pressure fed, and to contain the total mass of propellant need to ensure the required Δv. In order to estimate the magnitude of the complete pressure cascade, the difference of pressure across the injectors has been considered equal to the 30% of the chamber pressure, which is a generally accepted value for a preliminary sizing [21], moreover also a loss due to the fuel exiting the tank, $\Delta p_{dyn} = \frac{1}{2}\rho v^2$, has been taken into account. Thus, the tank nominal pressure will be:

$$p_{tank} = p_{chamber} + \Delta p_{inj} + \Delta p_{feed} + \Delta p_{dyn} \tag{4.18}$$

while the volume is equal to:

$$V_{tank} = \frac{m_{prop}}{\rho_{rho}} \tag{4.19}$$

each value is computed separately for the fuel and oxidizer tank.
Since the system is pressure fed, the sizing of the pressurizing Helium tank has been made considering the storage pressure equal to 200 *bar* at ambient temperature, plus a safety factor of 15% to consider loss due to the regulator and to the line till the pressurized tank. The total volume of gas has been computed in order to ensure, when fully discharged, a minimum pressure which is equal to the maximum required between the two propellant tanks (thanks to the regulator it won't be a problem to reduce it further).
The expansion has been considered adiabatic as follows:

$$p_S {V_{He}}^{\gamma} = p_T \left(V_{He} + V_{Ox} + V_{Fu}\right)^{\gamma} \tag{4.20}$$

where:

p_S is the storage pressure of the Helium when the tank is fully charged

V_{He} is the total volume of Helium

p_T is the fuel/oxidizer tank pressure

V_{Ox} and V_{Fu} refers to the fuel and oxidizer volumes

The previous equation, if solved for V_{He} leads to:

$$V_{He} = \frac{V_{Ox} + V_{Fu}}{\left(\frac{p_S}{p_T}\right)^{\gamma} - 1} \tag{4.21}$$

and accordingly the mass results:

$$\begin{cases} \rho_{He} = \frac{p \cdot R}{T \cdot M_{mol}} & \text{according to the gas state equation} \\ m_{He} = \rho_{He} V_{He} \end{cases} \tag{4.22}$$

that leads to the following results:

Propellant	$p_{OX}[bar]$	$p_{FU}[bar]$	$m_{He}[kg]$	$V_{He}[m^3]$
N2H4/N2O4	17.93	17.96	2.349	0.0619
H2O2/RP-1	17.07	16.96	2.373	0.0625

Table 4.10: Tank data

4.8 Scaled versions

The following tables show a summary of the main properties of the scaled thrust versions (0.5× & 2×) of the nominal engine designs presented in the previous sections.
O/F ratio has been taken from the nominal case, as not to optimise a totally different engine but to perform a simple scalability analysis. From this data, other parameters derived from CEA code data will end up being equal to the nominal scale engine.
ϵ, CR, P_c, pressure losses ,and L^* are also fixed from the nominal design.

Toxic couple, 0.5× scale	
Thrust $[N]$	350
O/F	0.9347
$\dot{m_{Fu}}$ $[\frac{kg}{s}]$	0.0529
$\dot{m_{Ox}}$ $[\frac{kg}{s}]$	0.0494
D_{CC} $[m]$	0.044
$V_{CC}[cm^3]$	142.6
I_s[s]	348.6
m_{Fu}[kg]	139.17
m_{Ox}[kg]	130.08
$m_{He}[kg]$	2.349
$m_{P+He}[kg]$	271.59
$V_{Fu}[m^3]$	0.1381
$V_{Ox}[m^3]$	0.0897
$t_b[s]$	2631
$D_{inj,Fu}[mm]$	0.98
$D_{inj,Ox}[mm]$	1.20
N_{Fu}	4
N_{Ox}	2*
$FinalT_{Fu}[K]$	459*
$FinalT_{Ox}[K]$	303
$A_t[m^2]$	$1.9 \cdot 10^{-4}$
$L_{Nozzle}[m]$	0.242
$v_{inj}^{Fu}[\frac{m}{s}]$	17
$v_{inj}^{Ox}[\frac{m}{s}]$	14

Toxic couple, 2× scale	
Thrust $[N]$	1400
O/F ratio	0.9347
$\dot{m_{Fu}}$ $[\frac{kg}{s}]$	0.2115
$\dot{m_{Ox}}$ $[\frac{kg}{s}]$	0.1977
D_{CC} $[m]$	0.088
$V_{CC}[cm^3]$	570.4
I_s[s]	348.6
m_{Fu}[kg]	139.17
m_{Ox}[kg]	130.08
$m_{He}[kg]$	2.349
$m_{P+He}[kg]$	271.57
$V_{Fu}[m^3]$	0.1381
$V_{Ox}[m^3]$	0.0897
$t_b[s]$	658
$D_{inj,Fu}[mm]$	0.81
$D_{inj,Ox}[mm]$	0.82
N_{Fu}	24
N_{Ox}	18
$FinalT_{Fu}[K]$	411
$FinalT_{Ox}[K]$	293
$A_t[m^2]$	$7.6 \cdot 10^{-4}$
$L_{Nozzle}[m]$	0.484
$v_{inj}^{Fu}[\frac{m}{s}]$	17
$v_{inj}^{Ox}[\frac{m}{s}]$	14

Table 4.11: Design parameters of 0.5× and 2× toxic fuel engines

Green couple, 0.5× scale	
Thrust $[N]$	350
O/F ratio	5.0916
$\dot{m_{Fu}}$ $[\frac{kg}{s}]$	0.0183
$\dot{m_{Ox}}$ $[\frac{kg}{s}]$	0.0930
D_{CC} $[m]$	0.04322
$V_{CC}[cm^3]$	268.67
I_s[s]	320.42
m_{Fu}[kg]	49.87
m_{Ox}[kg]	253.92
$m_{He}[kg]$	2.363
$m_{P+He}[kg]$	306.156
$V_{Fu}[m^3]$	0.06234
$V_{Ox}[m^3]$	0.1767
$t_b[s]$	2728
$D_{inj,Fu}[mm]$	0.871
$D_{inj,Ox}[mm]$	5.630
N_{Fu}	2*
N_{Ox}	4
$FinalT_{Fu}[K]$	439
$FinalT_{Ox}[K]$	431*
$A_t[m^2]$	$1.834{\cdot}10^{-4}$
$L_{Nozzle}[m]$	0.2373
$v_{inj}^{Fu}[\frac{m}{s}]$	19
$v_{inj}^{Ox}[\frac{m}{s}]$	14
Coating thickness $[mm]$	0.173

Green couple, 2× scale	
Thrust $[N]$	1400
O/F ratio	5.0916
$\dot{m_{Fu}}$ $[\frac{kg}{s}]$	0.0731
$\dot{m_{Ox}}$ $[\frac{kg}{s}]$	0.3722
D_{CC} $[m]$	0.0864
$V_{CC}[cm^3]$	1034
I_s[s]	320.42
m_{Fu}[kg]	49.87
m_{Ox}[kg]	253.92
$m_{He}[kg]$	2.41
$m_{P+He}[kg]$	306.20
$V_{Fu}[m^3]$	0.06234
$V_{Ox}[m^3]$	0.1767
$t_b[s]$	682
$D_{inj,Fu}[mm]$	0.821
$D_{inj,Ox}[mm]$	5.313
N_{Fu}	9
N_{Ox}	18
$FinalT_{Fu}[K]$	419
$FinalT_{Ox}[K]$	360
$A_t[m^2]$	$7.336{\cdot}10^{-4}$
$L_{Nozzle}[m]$	0.4745
$v_{inj}^{Fu}[\frac{m}{s}]$	19
$v_{inj}^{Ox}[\frac{m}{s}]$	14
Coating thickness $[mm]$	0.198

Table 4.12: Design parameters of 0.5× and 2× green fuel engines

In these tables the highlighted values, marked with the symbol "*", accounts for critical design states, found especially for the smaller engine case. For this particular case of study is highly suggested to use a ceramic shield layer to partially solve the temperature problem in the small toxic engine, since in the model simulated it is not implement, while the green one is actually a very critical design given the fact that it already considers it. In this case a solution could consist in reducing the expansion ratio to increase the propellant mass flow rate but, even in this way, it is not possible to solve the problem without having a very poor I_{SP}.

The '*' in the injectors number instead, represent a non optimal condition since it is too small number to allow a proper and effective mixing during the injection.

Chapter 5

Discussion

5.1 Different Design Comparison

The analysis performed is to be considered a preliminary one, as many uncertainties are evident and further research on the topic of small scale liquid rocket engines and on the performances of green fuels should be conducted.

However, what appears from the results of the simulation of the nominal thrust engines is that green propellants can be a competitive alternative in missions that do not require the best performance possible: in this cases, the small drop in performance and increase in propellant weight can be balanced by the lower cost of the propellant and its associated handling costs when compared to hydrazine.

5.2 Scalability

The goal of scaling the engine size, and therefore thrust, to smaller or larger values is to expand the number of alternatives on the catalogue while maintaining design costs to a minimum.
For the engine designs proposed in this paper the scalability analysis is based on the data provided by tables 4.11, 4.12 This is shown to be possible and straightforward in the $2\times$ scale, as dimensional errors due to additive manufacturing become less relevant and cooling performances are improved due to the quicker increase in propellant mass flow rate compared to the increase in surface to be cooled.
Scalability in this case can easily be implemented for both propellants, allowing even for more optimal O/F ratios to be used, which would not be feasible in the nominal scale due to a too high heat flux, which could not be removed purely by regenerative cooling.

On the other hand, scaling the nominal engines down to a smaller scale is not as straightforward, due to the decrease in the total injector area, which would either cause holes that are too small to reliably print with AM or too few holes which may cause improper burning of the propellants due to poor mixing.
Another big issue in miniaturization is the topic of heat management, as the area to be cooled decreases at a slower rate than the mass flow rate used to provide the cooling. In this situation other forms of heat management should be considered, such as implementing film cooling into the cooling strategy.
This option however, require significant modifications to the design or the production

process of the down-scaled engine, reducing the benefit of reusing the nominal design at a different scale.

For this reason it would be more feasible to design an engine from scratch for this kind of applications, keeping in mind the possible issues of cooling and feature size right from the beginning.

5.3 Monte Carlo Analysis

Current additive manufacturing techniques cannot yet guarantee the same level of dimensional accuracy of traditional manufacturing. In particular, this effect can be significant, as small manufacturing defects can have significant impacts on the real size of the injection holes, discharge coefficient C_d of the injectors, and on the throat area.

Mathematical analysis were performed, comparing the theoretical nominal engine performance considering a gaussian distribution of the areas of the elements of the injector plate with a $1\sigma = \pm 50\mu m$, the throat area with a $1\sigma = 1\%$, the expansion ratio with a $1\sigma = 1\%$, and a uniform distribution within ± 0.1 for the C_d, centered around the nominal value.
From these, engine main performance parameters and their distributions have been computed and reported in tab 5.3.
Notice that *perc.* accounts for Percentile, it represent the value at the corresponding percentile in the full set of data.

		Average	10 perc.	90 perc.
Toxic couple	$I_s[s]$	348	345.6	349.3
	$\Delta V[\frac{m}{s}]$	2495	2478	2505
	O/F	1.03	0.76	1.13
	Thrust [N]	739.9	624.2	772.1
	$T_{FU}[K]$	444	410	467
	$T_{OX}[K]$	281	295	297
Green couple	$I_s[s]$	316.5	310.4	323.1
	$\Delta V[\frac{m}{s}]$	2470	2422	2521
	O/F	4.57	4.15	6.26
	Thrust [N]	618.0	621.6	760.4
	T_{FU}	413	381	499
	T_{OX}	387	377	394

Table 5.1: Results of Montecarlo analysis

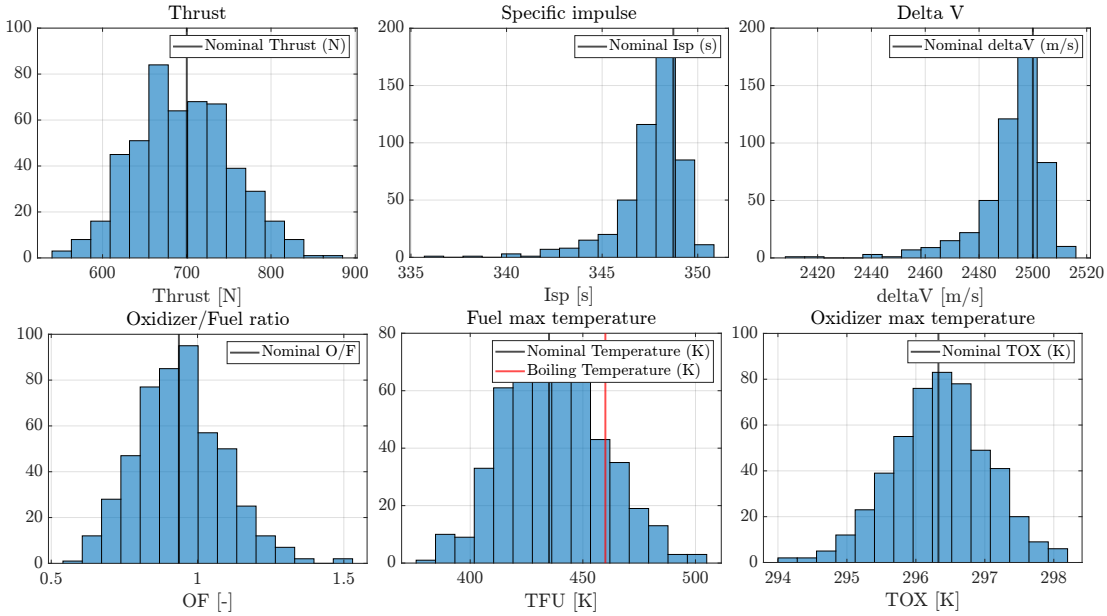

Figure 5.1: Performance variations for the nominal thrust Toxic couple engine

A slight change in those values can change significantly the final results. The thrust and OF vary by ±15% but still stay around their respective nominal values of 700N and 0.9. As for the fuel temperature, for some cases the maximum temperature is above its boiling temperature. Regarding the ΔV, the average value is slightly lower than the nominal one of 2500 m/s, and as such a safety factor shall be added to account for off-nominal performance related to dimensional accuracy.

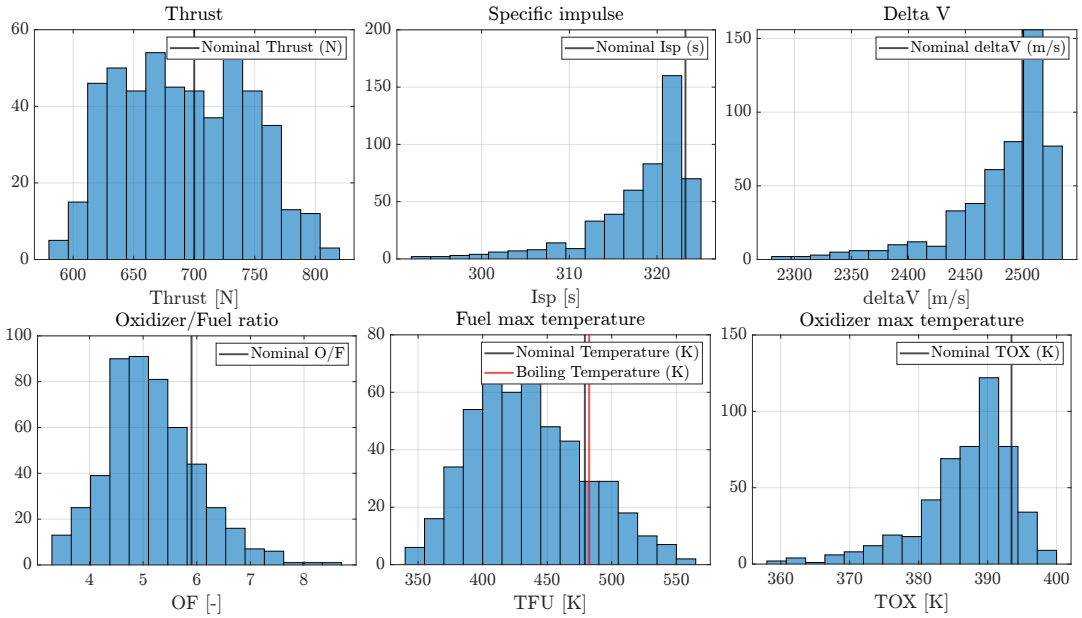

Figure 5.2: Performance variations for the nominal thrust Green couple engine

Moreover, the effects of those uncertainties also in the non nominal versions of the engines were analyzed. The results share the same pattern of the nominal engine ones, the following tables report the characterizing parameters.

		Average	10 perc.	90 perc.
Small scale	$I_s[s]$	356.45	342.15	349.08
	$\Delta V[\frac{m}{s}]$	2484	2453	2503
	O/F	0.9710	0.7248	1.2759
	Thrust [N]	348.29	304.39	393.50
	$T_{FU}[K]$	483	438	530
	$T_{OX}[K]$	316	314	318
Large scale	$I_s[s]$	346.53	344.89	349.11
	$\Delta V[\frac{m}{s}]$	2485	2459	2503
	O/F	0.7885	0.7050	1.2300
	Thrust [N]	1587	1223	1613
	T_{FU}	378	373	439
	T_{OX}	293	292	294

Table 5.2: Non nominal toxic engines

		Average	10 perc.	90 perc.
Small scale	$I_s[s]$	317.51	308.1	322.9
	$\Delta V[\frac{m}{s}]$	2477	2403.	2519
	O/F	5.102	4.0253	6.280
	Thrust [N]	346.56	312.19	381.23
	$T_{FU}[K]$	442	383	512
	$T_{OX}[K]$	442	428	452
Large scale	$I_s[s]$	317.9	308.7	323.13
	$\Delta V[\frac{m}{s}]$	2480	2408	2521
	O/F	5.205	4.044	6.381
	Thrust [N]	1398	1255.4	1538.60
	T_{FU}	426	370	486
	T_{OX}	374	365	379

Table 5.3: Non nominal green engine

As can be seen, even if the general performances are quite similar, smaller engines outperform over heating problems that reduce by increasing the thrust and consequently the propellant mass flow rate.

Chapter 6

Conclusion

In conclusion, for upper stages and liquid apogee kick motors that do not require the maximum performance available in terms of specific impulse, green propellants such as H2O2/RP-1 can be a suitable alternative, reducing costs related to the handling of extremely toxic propellants. If instead, maximizing the performances is the objective, the toxic propellant (H2O2/H2O4) shows the best behaviour.

Relating to the topic of additive manufacturing, the level of maturity of current state-of-the-art metal printers is suited to medium-high thrust levels, as they currently lack the precision and tolerances required by smaller scale engines. They do however show some strengths in the aspect of per-unit production costs and complexity.

Scalability to small sizes shows criticalities in terms of cooling when pure regenerative cooling, or even considering a coating layer, is taken into account, but further improvements in high temperature, printable metallic alloys may allow for the production of entirely 3D printed combustion chamber-case assemblies even at these scales in the future.
Temporary solutions for the production of this class of high performance, low thrust engines requires the use of different techniques to mitigate the problem of heat management. Even in the nominal size, the use of a coating is strongly suggested, especially in the green propellant design, to ensure proper thermal behaviour of the system.

In general, propulsion system design shall take into account a safety factor for the total mission ΔV, as the Montecarlo analyses (5.3) show a tendency to achieve a lower I_s than the nominal design case.

Bibliography

[1] European Space Agency. *ESA - Vesratile, green rocket engine gets go-ahead from ESA*. https://www.esa.int/Enabling_Support/Space_Transportation/Future_space_transportation/Versatile_green_rocket_engine_gets_go-ahead_from_ESA.

[2] Paweł Surmacz. "Green rocket propulsion research and development at the institute of aviation: problems and perspectives". In: *Journal of KONES powertrain and Transport* 23 (2016).

[3] Stefania Carlotti and Filippo Maggi. "Evaluating new liquid storable bipropellants: Safety and performance assessments". In: *Aerospace, 9(10):561* (2022).

[4] Jan Kindracki Adam Okninski. "Multidisciplinary optimisation of bipropellant rocket engines using H2O2 as oxidiser". In: (2018).

[5] Dr. Robert Lechler. *Literature Survey of Materials compatible with Propellants*. Tech. rep. Salt Lake City, UT: Institute of Space Propulsion, Oct. 2015.

[6] P. E. Uney and D. A. Fester. *MATERIAL COMPATIBILITY WITH SPACE STORABLE PROPELLANTS DESIGN HANDBOOK*. Denver, Colorado: Martin Marietta corporation, 1972.

[7] *CHEMICAL COMPATIBILITY CHART Metallic Materials Used in Bal Seal Products*. Tech. rep. TR-60C. BAL SEAL Engineering.

[8] W. K. Boyd. *COMPATIBILITY OF MATERIALS WITH ROCKET PROPELLANTS AND OXIDIZERS*. Tech. rep. AD-613 553. Colombus, Ohio: Battelle Memorial Institute, Jan. 1963.

[9] L. Ordonez Valles et al. *Challenges and Opportunities of Green Propellants and Electric Pump Feeding for Future European Kick Stages*. https://doi.org/10.1007/s42496-022-00133-6.

[10] *HYDROGEN PEROXIDE HANDBOOK*. Tech. rep. AFRPL-TR-67-144. Canoga Park, California: Chemical and Material Sciences Department Research Division Rocketdyne, a Division of North American Aviation, Inc., July 1967.

[11] G. S. Gill et al. *LIQUID ROCKET ENGINE INJECTORS*. Tech. rep. NASA SP-8089. Cleveland, Ohio: NASA, Mar. 1976.

[12] J. R. Wooten and P. T. Lansaw. *HIGH-TEMPERATURE, OXIDATION-RESISTANT THRUSTER RESEARCH*. Tech. rep. NAS3-24643. Cleveland, Ohio: NASA, Feb. 1990.

[13] SLM Solutions. *Mid and High Volume Metal Additive Manufacturing, SLM Solutions*. https://www.slm-solutions.com/products-and-solutions/machines/slm-280/.

[14] Di Wang et al. “Design and Fabrication of a Precision Template for Spine Surgery Using Selective Laser Melting (SLM)”. In: *Materials, 9(7):608* (2016).

[15] Visvaldis Svinka Ludmila Mahnicka-Goremikina Ruta Svinka. “Thermal Properties of Porous Mullite Ceramics Modified with Microsized ZrO2 and WO3”. In: (2022), p. 18.

[16] Huang Huzel. *Design of Liquid Propellant Rocket Systems.*

[17] Roberts Koopmans Shrimpton. “Dependence of Pellet Shape and Size on Pressure Drop in H2O2 Thrusters”. In: (2014), p. 15.

[18] Paweł Surmacz. “GREEN ROCKET PROPULSION RESEARCH AND DEVELOPMENT AT THE INSTITUTE OF AVIATION: PROBLEMS AND PERSPECTIVES”. In: *Journal of KONES* (2016).

[19] Adam Okninsk Wioleta Kopacz. “Hydrogen peroxide – A promising oxidizer for rocket propulsion and its application in solid rocket propellants”. In: (2022).

[20] Ronald W. Humble and Gary N. Henry. *Space Propulsion Analysis And Design.* The McGraw-Hill Companies, 1995.

[21] Rochester Institute of Technology. *Injector Overview.* `http://edge.rit.edu/edge/P18102/public/Engine%20Specifications/Propulsion/Injector/Injector`.

[22] Brian A. Sweeney. *Like-Doublet Injectors : the effects of varying the impingement distance and an analysis of the primary atomization one.* Tech. rep. 2016.

[23] *Bulkperoxide.* `https://bulkperoxide.com/is-it-safe-to-heathydrogen-peroxide/#:~:text=The%20hydrogen%20peroxide%20which%20is,which%20they%20start%20to%20decompose`.

[24] Engineering ToolBox. *Roughness Surface Coefficients.* `https://www.engineeringtoolbox.com/surface-roughness-ventilation-ducts-d_209.html`.

[25] ArianeGroup. *Propellant and Pressurant Valves for Spacecraft Propulsion Systems.* `https://www.space-propulsion.com/spacecraft-propulsion/valves/index.html`.